A Self-Consistent Field Quantum Hydrodynamic Approach for Molecular Clusters†

Sean W. Derrickson* and Eric R. Bittner

Department of Chemistry, University of Houston, Houston, Texas 77204

Received: October 14, 2005; In Final Form: January 16, 2006

We present a novel self-consistent orbital-free method useful for quantum clusters. The method uses a hydrodynamical approach based on the de Broglie−Bohm description of quantum mechanics to satisfy an orbital-free density functional-like Euler−Lagrange equation for the ground state of the system. In addition, we use an information theoretical approach to obtain the optimal density function derived from a series of statistical sample points in terms of density approximates. These are then used to calculate an approximation to the quantum force in the hydrodynamic description. As a demonstration of the utility and flexibility of the approach, we compute the lowest-energy structures for small rare-glass clusters of argon and neon with 4, 5, 13, and 19 atoms. Extension to more complex systems is straightforward.

I. Introduction

Atomic and molecular clusters provide almost ideal "laboratory" systems for studying quantum versus classical dynamical and structural effects as a function of the size and scale of a given system. Such considerations are important especially because the transition from microscopic to macroscopic (bulk) is not always smooth. For instance, theoretical results indicate a "coexistence region" of the liquid and solid phases in some clusters[1−4] and that quantum effects may suppress surface melting in certain-sized clusters.[5] Rare gas systems provide a simple and effective way to study the underlying physics of these transitions.[5−7] Rare gas clusters and liquids are easily enough modeled with classical molecular dynamics simulations; however, treating the quantum dynamics of even small-sized systems remains a formidable challange. Quantum corrections are important even in equilibrium calculations and finite temperature calculations because the quantum character strongly affects the thermodynamics via changes in the ground-state structure due to increasing zero-point energies.[8] Quantum corrections have been shown to lower solid-to-liquid transition temperatures by approximately 10%, and the zero-point energy for small clusters can equal up to 35% of the classical binding energy, defined as the total potential energy divided by the number of atoms.[9] In light of these facts, the de Boer parameter, Λ, can be used to determine the point at which quantum effects will significantly alter the thermodynamic properties of Lennard−Jones systems.[8−10]

Any Lennard−Jones system can be defined in terms of its potential depth ϵ, its length scale σ, and mass m. For a given set of parameters, the thermal de Broglie wavelength, $\lambda = \hbar/\sigma\sqrt{mk_BT}$, provides a means of approximating the quantum effects at some reduced temperature of the system, $T^* = k_BT/\epsilon$. Furthermore, taking the ratio of λ for two different sets of parameters provides a means of comparing the quantum effects of one system versus the other. This leads to the de Boer parameter, $\Lambda = \hbar/r_m\sqrt{m\epsilon}$.[11] In short, the de Boer parameter measures the delocalization of the system compared to its size. Λ has a classical limit of $\Lambda = 0$, and anything above $\Lambda \approx 0.3$ is considered a quantum system.

For these systems, one could utilize exact quantum mechanical methods, but it has long been recognized that the computational effort of grid-based quantum mechanical methods for nuclear dynamical problems grows exponentially with the number of degrees of freedom. This limits the size of systems that can be handled in an exact manner to those with four or fewer atoms. This is perhaps best illustrated in the field of reactive scattering calculations, which have been limited to systems with 6D[12−15] and in other areas such as photodissociation processes.[16,17] In light of this, considerable progress has been made in developing rigorous approaches for contracting the basis size required to perform such calculations.

One such approach that has seen considerable success is the multiconfigurational time-dependent Hartree approach (MCTDH) developed by Meyer and co-workers[18,19] that overcomes this limitation in a numerically exact way by expanding the time-dependent wave function in terms of a number of time-dependent configurations,

$$\Psi(t) = \sum_J A_J(t)\Phi_J(t)$$

in which the single-particle (or quasiparticle) basis functions $\Phi_J(t)$ and the expansion coefficients are coupled by the MCTDH equations of motion. Unfortunately, the MCTDH approach has difficulty with pairwise interactions, making it unsuitable for Lennard−Jones clusters.

For condensed phase systems, path integral Monte Carlo (PIMC) and centroid-based molecular dyamics remain the method of choice. These approaches have been extremely successful in calculating a wide variety of thermodynamic properties of heavily quantum systems.[8,10,20,21] A number of interesting results have emerged from these simulations. A notable example of these is the lattice expansions under constant pressure and temperature (NPT) conditions associated with the quantum effects, which have a large effect on the binding energy versus classical systems.[22] Despite the success of PIMC approaches of late, there are some inherent difficulties. For instance, at low temperatures, the number of parameters that must be included can become prohibitive and lead to slow

† Part of the special issue "John C. Light Festschrift".

* Corresponding author. E-mail: sderrick@mail.uh.edu.

10.1021/jp055889q CCC: $33.50
Published on Web 02/15/2006

convergence. Also, the computational complexity is increased by the extra degrees of freedom that arise in PIMC-derived simulations.[8]

We present an approach that is appropriate for low-temperature Lennard−Jones clusters and that will shed new light on the origin and character of the quantum effects seen in these systems. The method we will outline begins with the assumption that the configurational density $n(\mathbf{r}_1,\cdots,\mathbf{r}_N)$ that describes the statistical likelihood of finding the system in a given multidimensional configuration $\{\mathbf{r}_1\cdots\mathbf{r}_N\}$ can be written as a superposition of statistical approximates $p(\mathbf{r}_1\cdots\mathbf{r}_N, c_m)$. These are the joint probabilities for finding the system at $\{\mathbf{r}_1\cdots\mathbf{r}_N\}$ and that the configuration is a variant of some statistical distribution described by the approximate. These approximates can be any elementary probability density function that can be specified in terms of its statistical moments, c_m. The simplest of these for our purposes are multidimensional Gaussians. We then use a Bayesian analysis to deduce from a statistical sampling of the density the best set of m statistical approximates describing that density.[23] In addition, the algorithm also utilizes a *grid-free* adaptive hydrodynamic approach for the relaxing of the sample points that make up a statistical sampling of the density. These are eventually relaxed to the quantum ground-state density for the system of N nuclei.

The approach is similar in some respects to hydrodynamic density functional theory (DFT), which is the basis for time-dependent density functional theories.[24,25] Hydrodynamic DFT has been used to calculate, among other quantities, response functions in large systems and second-order terms in the perturbation theory for many electron systems.[26,27] By taking variations in the energy functional with respect to the density and the current density, an Euler−Lagrange equation and a continuity equation can be derived. These give the equations of motion for the electron density. Under a time-independent Hamiltonian, one is left with the Euler equation of static DFT, similar to what we obtain.

As proof of concept, we will present the details of the ground vibrational energy of small clusters of argon and neon. For argon, the de Boer parameter is $\Lambda \approx 0.03$. This corresponds to an essentially classical system, and quantum effects can be treated as a perturbation. For neon, $\Lambda \approx 0.1$, indicating that neon is a *quasiquantum* system. It is expected that the method proposed will provide a useful way of determining any changes in structure due to quantum effects such as zero-point energy and tunneling. We confine the method at present to zero temperature. Finally, we will discuss the results obtained. Because the work at present is intended to illustrate the usefulness of the method and not to compare to any benchmark simulations, we compare our results to simple classical results. We will also show how the approach we have outlined may be used to develop new quantum-classical approaches for treating quantum mechanical solute particles (such as an excess e^- or He atom) in a liquid of classical or quasiclassical atoms (such as Ar or Ne).

II. Theoretical Development

We begin by writing the full many-body Hamiltonian for the nuclear motion of a collection of atoms with pairwise interaction potentials (atomic units are used throughout),

$$H = -\sum_{i=1}^{N} \frac{1}{2m_i}\nabla_i^2 + \sum_{i\neq j} V(ij) \tag{1}$$

Corresponding to this, for an arbitrary N-body trial density, the energy functional is given by

$$E[n] = T[n] + \sum_{i\neq j} \int n_i(\mathbf{r}) n_j(\mathbf{r}) V(ij)\, \mathrm{d}\mathbf{r} \tag{2}$$

We have assumed that the density is separable into atomic components, i.e.,

$$n(1, \cdots, N) = \prod_{i=1}^{N} n_i(\mathbf{r}) \tag{3}$$

To reduce confusion, unless otherwise stated, all densities used for the remainder of this work are separable "atomic" densities.

From the form of the kinetic energy operator, the kinetic energy functional will also be a sum of individual functionals:

$$T[n(1\cdots N)] = \sum_{i=1}^{N} T_i[n_i(\mathbf{r})] \tag{4}$$

As in electronic structure DFT, evaluating the kinetic energy functionals in an orbital-free form is problematic because the quantum kinetic energy operator is a nonlocal operator and the density is a local function.[28]

If we write the quantum wave function in polar form, as in the hydrodynamic formulation of quantum mechanics,[29−31]

$$\Psi(1\cdots N) = \sqrt{n(1\cdots N)}\, e^{i\phi(1\cdots N)} \tag{5}$$

we can arrive at a stationary condition for the hydrodynamic description if $\nabla\phi = 0$[32], which, assuming single-particle densities is

$$V(1\cdots N) - \sum_i \frac{1}{2m_i}\frac{1}{\sqrt{n_i(\mathbf{r})}}\nabla_i^2\sqrt{n_i(\mathbf{r})} = \text{const} \tag{6}$$

The first term on the left-hand side is the external potential. The second is the quantum potential from the de Broglie−Bohm or hydrodynamic formulation,[33−36] which we shall notate as Q. The constant is the energy for the stationary state of the system. For stationary states, the forces from these potentials exactly counterbalance each other[53]

$$\nabla Q + \nabla V = 0 \tag{7}$$

By multiplying by the density (eq 3), the integrated form of eq 6 gives a form for the kinetic energy functional in eq 4 as,

$$T[n_i(\mathbf{r})] = -\frac{1}{2m_i}\int \sqrt{n_i(\mathbf{r})}\nabla_i^2\sqrt{n_i(\mathbf{r})}\, \mathrm{d}\mathbf{r} \tag{8}$$

Integrating by parts and letting $n_i \rightarrow 0$ at $\pm\infty$ produces the familiar von Weizsacker kinetic energy functional[37]

$$T_W[n_i(\mathbf{r})] = +\frac{1}{8m}\int \frac{1}{n_i(\mathbf{r})}\nabla_{\bar{i}} n_i(\mathbf{r})\cdot\nabla_{\bar{i}} n_i(\mathbf{r})\, \mathrm{d}\mathbf{r} \tag{9}$$

Thus, the total energy functional is given in terms of the single-particle densities as,

$$E[n] = \sum_{i=1}^{N} T_W[n_i(\mathbf{r})] + \sum_{i\neq j}\int n_i(\mathbf{r}) n_j(\mathbf{r}) V(ij)\, \mathrm{d}\mathbf{r} \tag{10}$$

Taking the variation of $E[n]$ with respect to the single-particle

densities with the constraint that $\sum_i \int n_i(\mathbf{r})\, d\mathbf{r} = N$ (or $\int n_i(\mathbf{r})\, d\mathbf{r} = 1$),

$$\delta\{\sum_{i=1}^{N} (T_W[n_i(\mathbf{r})] + \sum_{j\neq i} \int n_i(\mathbf{r}) n_j(\mathbf{r}) V(ij)\, d\mathbf{r} - \mu_i(\int n_i(\mathbf{r})\, d\mathbf{r} - 1))\} = 0 \quad (11)$$

leads to the following Euler−Lagrange equations:

$$\frac{\delta T_W[n_i(\mathbf{r})]}{\delta n_i(\mathbf{r})} + \sum_{j\neq i} \int V(ij) n_j(\mathbf{r})\, d\mathbf{r} - \mu_i = 0 \quad (12)$$

When satisfied, $\mu = \sum_i \mu_i$ is a stationary vibrational-state energy, and the $n_i(\mathbf{r}) = |\phi_i(\mathbf{r})|^2$ are the probability densities of the individual nuclei.

Let us take a simple pedagogic case of a particle in a harmonic well, taking the trial density to be a Gaussian, $n(x) = \sqrt{a/\pi}\exp(-ax^2)$. Evaluating the energy functional yields:

$$E[n(x)] = \frac{1}{4m}a + \frac{m\omega^2}{4a}$$

Minimizing with respect to the trial density,

$$\frac{\delta E[n]}{\delta n} = \frac{dE}{da} = 0$$

yields the familiar $E = \omega/2$ and $a = m\omega$. This idea is easy to extend beyond purely harmonic systems and Gaussian trial functions. Because $n_i(\mathbf{r})$ is a probability density function, it is a positive, real, and integrable function.

In the following section, we show how the single-particle densities can be estimated as superpositions of single-particle density approximates based upon a statistical sampling of the densities.

III. Mixture Modeling

Consider an ensemble of sample points, $\mathbf{R} = \{\mathbf{r}_1,...,\mathbf{r}_K\}$, that statistically represents a multidimensional quantum probability density. The corresponding probability density function (PDF) can be represented by a mixture model[38,39] by summing a finite number M of density approximates. This is expressed as a sum over joint probabilities,

$$n(\mathbf{r}) = \sum_{m}^{M} p(\mathbf{r}, c_m) \quad (13)$$

where $p(\mathbf{r}, c_m)$ is the probability that a randomly chosen member of the ensemble has the configuration $\mathbf{r}$ and is a variant of the mth approximate designated by c_m. These approximates may be Gaussians or any other integrable multidimensional function that can be parametrized by its moments. For Gaussian clusters, we have a weight $p(c_m)$, a mean position vector μ_m, and a covariance matrix $\mathbf{C}_m$.

The assumption that the density can be split into a sum of approximates is exact in the limit of infinite approximates. In general, one looks for the smallest number of approximates necessary to describe the system of interest. We know that, for a Gaussian density packet on a parabolic surface, only one approximate is needed and is exact. For the present system, we assume that, for the ground state, the densities remain confined near the bottom of the Lennard−Jones potential well. Please note that the formation of nodes will not be problematic as in dynamical simulations because we are limited to eigenstates and, in particular, the ground state. The ground state is rigorously node free for bosonic systems. Consequently, we expect that, at most, only a few Gaussian approximates will be needed for the ground-state calculation.

The number of parameters needed to describe the approximates is directly related to the physical assumptions made about the system. If we assume that the Gaussian components for each atom are separable, then we only need to be able to specify $m(3N(3N + 1)/(2 + 3N + 1)) = \mathcal{O}(mN^2)$ variables. These correspond to the elements of the covariance matrix, the central mean, and amplitude for m $3N$-dimensional Gaussians. Also, explicit correlations between various degrees of freedom can be excluded in a straightforward way by factoring the approximates that describe a particular atom. We can then expand the atomic density $n_i(\mathbf{r})$ as a linear combination of density approximates,

$$n_i(\mathbf{r}) = \sum_{m=1}^{M} p_{mi}(c_{mi}, \mathbf{r}) \quad (14)$$

for the i atoms of the system. This dramatically reduces the number of coefficients we need to determine to $mN \times (6 + 3 + 1) = \mathcal{O}(mN)$. Intermediate factorization schemes yield similar scaling behavior, allowing one to tune the computational complexity of the system depending upon the degree of correlation required by a particular physical problem. For example, one can define *quasi-atoms* by explicitly including covariance between the degrees of freedom of two or more atoms.

By definition, each joint probability in eq 13 is related to a pair of conditional probabilities according to the relation

$$p(\mathbf{r}, c_m) = p(c_m)p(\mathbf{r}|c_m) = n(\mathbf{r})p(c_m|\mathbf{r}) \quad (15)$$

where the forward conditional probability $p(\mathbf{r}|c_m)$ refers to the probability that a randomly chosen variant of c_m has the $3N$ dimensional configuration $\mathbf{r}$. Conversely, the posterior probability $p(c_m|\mathbf{r})$ refers to the probability that the configuration point $\mathbf{r}$ is a variant of the approximate c_m. In probability theory, $n(\mathbf{r})$ and $p(c_m)$ are known as marginal probabilities; however, we shall simply refer to them as the quantum density and weight of the mth approximate, respectively. The expansion weights, $p(c_m)$, are strictly positive, semidefinite, and sum to unity. By substituting the first equality of eq 15 into eq 13, we have,

$$n(\mathbf{r}) = \sum_{m}^{M} p(c_m)p(\mathbf{r}|c_m) \quad (16)$$

We have considerable freedom at this point in specifying the exact functional form of the conditional probabilities as well as the degree of correlation within each conditional. This freedom of specification allows us to construct "models" that explicitly take into account nonseparable correlations in configuration space. For the case of Gaussian approximates, this is accomplished by keeping or discarding various off-diagonal terms incorporated in the covariance matrix, $\mathbf{C}$,

$$p(\mathbf{r}|c_m) = \sqrt{\frac{||\mathbf{C}_m^{-1}||}{(2\pi)^{3N}}}\, e^{-(\mathbf{r}_d-\mu_{m,d})^T\cdot\mathbf{C}_m^{-1}\cdot(\mathbf{r}_d-\mu_{m,d})} \quad (17)$$

$||\mathbf{C}_m^{-1}||$ is the reciprocal of the greatest value of the determinant of the covariance matrix, and the subscript indicates that this is the covariance matrix corresponding to the mth approximate.

If the covariance matrix is real and symmetric, then it is possible to construct a model that assumes that each approximate is completely separable and takes the form of a product over the $3N$-dimensional configuration space. In this case, the covariance matrix, $\mathbf{C}_m$, reduces to a variance vector, $\sigma^2_{m,d}$, and the forward conditional probability becomes

$$p(\mathbf{r}|c_m) = \prod_d^{3N} \sqrt{\frac{1}{2\pi\sigma^2_{m,d}}}\, e^{-((\mathbf{r}_d-\mu_{m,d})^2/(2\sigma_{m,d}^2))} \tag{18}$$

Numerical tests by Maddox and Bittner indicate that the separable case is computationally faster for high-dimensional systems, but produces a less-accurate estimate of the quantum ground-state energy.[23] For larger systems, the separable case will certainly speed up calculations. As expected, there is a direct connection between the covariance matrix form and the form of the density assumed in eq 3. We also note that it is feasible to construct any combination of covariant and separable degrees of freedom if there is some reason to do so on the basis of the symmetry of any physical problem. For a discussion of the strengths and weaknesses involved with mixture models, one is referred to refs 23, 40.

Once a model is decided upon, one must then determine the parameters, in this case, the Gaussian parameters $p(c_m)$, μ_m, and $\mathbf{C}_m$, for each approximate from the statistical points representing the density. For instance, the mean position vectors of the approximates are defined by the moments of the forward conditional probabilities,

$$\mu_m = \int \mathbf{r} p(\mathbf{r}|c_m)\, \mathrm{d}\mathbf{r} \tag{19}$$

By rearranging eq 15 and substituting into eq 19, we can write this as

$$\mu_m = \int \mathbf{r} \frac{n(\mathbf{r})p(c_m|\mathbf{r})}{p(c_m)}\, \mathrm{d}\mathbf{r} \tag{20}$$

This is easily approximated by taking a Monte Carlo integration over the ensemble of points $\{\mathbf{r}_k\}$ sampled from the $n(\mathbf{r})$ PDF,

$$\mu_m \approx \frac{1}{Kp(c_m)} \sum_k^K \mathbf{r}_k p(c_m|\mathbf{r}_k) \tag{21}$$

We also define similar expressions for both the covariance matrix and the expansion weights in the following:

$$p(c_m) \approx \frac{1}{K} \sum_k^K p(c_m|\mathbf{r}_k) \tag{22}$$

$$\mathbf{C}_m \approx \frac{1}{Kp(c_m)} \sum_k^K (\mathbf{r}_k - \mu_m)(\mathbf{r}_k - \mu_m)^T p(c_m|\mathbf{r}_k) \tag{23}$$

For the case of separable approximates, the variances are given by the diagonal elements $\sigma^2_{m,i} = (\mathbf{C}_m)_{ii}$. The posterior terms $p(c_m|\mathbf{r}_k)$ for each $\mathbf{r}_k$ sample point in eqs 21−23 are evaluated directly from the forward probabilities according to Bayes' equation,

$$p(c_m|\mathbf{r}_k) = \frac{p(c_m)p(\mathbf{r}_k|c_m)}{\sum_m p(c_m)p(\mathbf{r}_k|c_m)} \tag{24}$$

Within this viewpoint, the sample points can be considered to be a data set that represents the results of a series of successive measurements. Each data point carries an equal amount of information describing the underlying quantum probability density function. Bayes' equation gives the ratio of how well a given approximate describes $\mathbf{r}_k$ to how well $\mathbf{r}_k$ is described by all of the approximates. Thus, it represents the fraction of explanatory information that a given sample point gives to the mth approximate. The approximate that *best* describes the point will have the largest posterior probability at that point. Equations 21−24 can be iterated self-consistently in order to determine the best possible set of parameters that describe $n_i(\mathbf{r})$ in terms of a given ensemble of data points. In doing so, we effectively maximize the log-likelihood that the overall density model describes the entire collection of data points,

$$L = \log \prod_k n(\mathbf{r}_k)$$

Taking the variation of L with respect to the model parameters generates a series of update rules for moving the approximates through parameter space in the direction along $\nabla_{\bar{c}_m} L$.[38] For the case of Gaussian approximates, the update rules for the mean, covariance matrix, and marginal probabilities are given by,

$$\delta\mu_m = \frac{\mathbf{C}_m}{Kp(c_m)} \nabla_{\bar{\mu}_m} L$$

$$\delta\mathbf{C}_m = \frac{2(\mathbf{C}_m \otimes \mathbf{C}_m)}{Kp(c_m)} \nabla_{\bar{\mathbf{C}}_m} L$$

$$\delta p(c_m) = \frac{1}{K}(\mathrm{diag}[\Omega] - \Omega(\Omega)^T)\nabla_{\bar{\Omega}} L$$

Where $\otimes$ is the Kronecker product, Ω is the vector of all expansion weights, $\Omega = [p(c_1),..., p(c_m)]^T$, and diag[$\Omega$] is a matrix with the elements from Ω constituting the diagonal entries.[41]

We will now show how the coefficients (rather moments) of the approximates can be optimized to compute both the ground-state energy and ground-state single-particle densities.

IV. Relaxing the Sample Points

The next step in our approach is to generate the appropriate equations of motion to evolve the sample points either in real or imaginary time. The quantum Hamilton−Jacobi equation generates the equations of motion for the ray-lines of a time-dependent solution to the Schrödinger equation.[33−36]

$$\frac{\partial S}{\partial t} + \sum_i \frac{|\nabla_{\bar{i}} S|^2}{2m_i} + \sum_{i\neq j} \int n_i(\mathbf{r}) n_j(\mathbf{r}) V(ij)\, \mathrm{d}\mathbf{r} - \sum_i \frac{1}{2m_i} \frac{1}{\sqrt{n_i(\mathbf{r})}} \nabla_i^2 \sqrt{n_i(\mathbf{r})} = 0 \tag{25}$$

Because the density is separable into components, we easily arrive at a set of time-dependent self-consistent field equations whereby the motion of atom i is determined by the average potential interaction between atom i and the rest of the atoms

in the system,

$$\dot{S}(i) + \frac{|\nabla_{\vec{i}} S|^2}{2m_i} + \sum_{j \neq i} \int V(ij) n_j(\mathbf{r})\, d\mathbf{r} - \frac{1}{2m_i} \frac{1}{\sqrt{n_i(\mathbf{r})}} \nabla_i^2 \sqrt{n_i(\mathbf{r})} = 0 \quad (26)$$

Taking $\nabla\vec{S} = \mathbf{p} = m_i\dot{\mathbf{r}}$ as a momentum of a particle, the equations of motion along a given ray-line or characteristic $\mathbf{r}_k(t)$ of the quantum wave function are given by

$$m_i \ddot{\mathbf{r}}_k = -\sum_{j \neq i} \int (\nabla\vec{V}(ij)) n_j(\mathbf{r})\, d\mathbf{r} - \nabla\vec{Q}[n_i(\mathbf{r})] \quad (27)$$

where $Q[n_i(\mathbf{r})]$ is the Bohmian quantum potential specified by the last term in eq 26. Recall in the last equation that the $\mathbf{r}_k$'s are the sample points that constitute the density for a given atom. Stationary solutions of the time-dependent Schrödinger equation are obtained whenever $m_i\ddot{\mathbf{r}}_k = 0$. Consequently, by iteratively relaxing the sample points in a direction along the energy gradient specified by

$$\nabla_{\vec{i}} E = -\sum_{j \neq i} \int (\nabla\vec{V}(ij)) n_j(\mathbf{r})\, d\mathbf{r} - \nabla\vec{Q}[n_i(\mathbf{r})] \quad (28)$$

one obtains a minimal energy self-consistent field density for the *i*th atom.

To calculate the ground vibrational-state energy of the system, we need to include an artificial damping to the Hamiltonian of the system. In this case, the total force on a particle at any given step is given by,

$$\dot{\mathbf{v}} = \mathbf{f}_q + \mathbf{f}_c - \gamma\mathbf{v} \quad (29)$$

where γ represents a small dissipative coefficient and $\mathbf{f}_q$, $\mathbf{f}_c$ are the forces arising from the quantum and mean-field forces given in eq 27 above. The damping causes some kinetic energy loss at each step in the simulation. For a classical case, the ensemble points would collapse to a δ function(s) centered about the minimum energy point(s) of the potential surface for the particle(s). For the present case, as the distribution narrows, the quantum force gets larger, forcing the ensemble to maintain some finite width. The sample points eventually converge to an equilibrium that corresponds to the ground-state quantum density from which the ground-state energy is derived.

This process is similar to the semiclassical approximation strategy for including quantum effects into otherwise classical calculations introduced by Garaschuk and Rassolov.[42,43] This semiclassical approximate methodology is based upon de Broglie−Bohm trajectories and involves the convolution of the quantum density with a minimum uncertainty wave packet that in turn is expanded in a linear combination of Gaussian functions

$$\rho(x) \approx f(x) = \sum_n c_n^2 \exp[-a_n^2(x - X_n)] \quad (30)$$

The Gaussian parameters $s = \{c_n, X_n, a_n\}$ in eq 30 are determined by minimizing the functional

$$F = \int [\rho(x) - f(x)]^2\, dx \quad (31)$$

using an iterative procedure that explicitly involves solving the set of equations $\partial F/\partial s_k = 0$. The parametrized density leads to an approximate quantum potential (AQP) that is used to propagate an ensemble of trajectories. This approach has been used successfully in computing reactive scattering cross-sections for the collinear $H + H_2$ reaction.

It is important at this point to recognize the numerical difficulties our group and others have faced in developing hydrodynamic trajectory-based approaches for time-dependent systems.[23,36,44−47] The foremost difficulty is in the accurate evaluation of the quantum potential from an irregular mesh of points.[44,46] The quantum potential is a function of the local curvature of the density and can become singular and rapidly varying as nodes form in the wave function or when the wave function is sharply peaked, i.e., when $n^{1/2} \rightarrow 0$ faster than $\nabla^2 n^{1/2} \rightarrow 0$. These inherent properties make an accurate numerical calculation of the quantum potential and its derivatives very difficult for all but the simplest systems. For a comprehensive discussion of different aspects regarding quantum trajectories and nodes, see refs 32, 48. These difficulties are avoided in the cluster model approximation of the density by using the expectation maximization (EM) algorithm.[23] By obtaining a global optimal function that describes the density, we can *analytically* compute the quantum force with great accuracy. The issue of nodes is essentially avoided so long as we are judicious in our choice of density approximates. If we choose node-free approximates, then our overall density will likewise be node free. For the purpose of determining vibrational ground-states, this seems to be a worthwhile compromise.

In summation, we will give a synopsis of the algorithm. We first initialize the system. This involves, for each atom, generating and sampling a normalized trial density $n_i(\mathrm{r})$. We then iterate through the following steps:

1. By using the EM routines and the given sample of points, compute the coefficients for the density approximates.

2. Compute the forces on each point by using eq 28 with eq 29 and advance each point along the energy gradient for one step. This generates a new sample of points describing the single-particle density for each atom. The new distribution should have a lower total energy since we moved the sample points in the direction toward lower energy.

3. Check for convergence and repeat if necessary.

V. Vibrational Ground State of Rare-Gas Clusters

As we discussed above, rare gas clusters provide a set of well-defined test cases for new quantum and mixed quantum-classical methods. Here, we focus our attention on determining the quantum equilibrium ground states for argon and neon clusters with up to 19 atoms. In the calculations presented here, we used 300 statistical points to represent the density of each atom and propagated the SCF equations described above until the energy and the density were sufficiently converged. Typically, this required 1.5−3 million cycles. Along the course of the energy minimization, we strongly damped the time evolution of the sample points to eliminate as much of the oscillations and breathing of the density components as possible.

The Lennard−Jones parameters for the argon clusters are $\epsilon = 0.9976$ kJ/mol and $\sigma = 3.42$ Å, and $\epsilon = 0.3059$ kJ/mol and $\sigma = 2.79$ Å for the neon clusters.[49] Initial configurations for the simulations are chosen to be close to the classical molecular dynamics minimum-energy geometry and are given some initial Gaussian spread.

We show in Figure 1 isodensity (0.006) contour plots for the Ar_4, Ar_5, Ne_4, and Ne_5, http://eiger.chem.uh.edu:8080/web-Mathematica/pchem-apps/Plot3DLive.jsp.[54] One can see quite clearly the underlying three-dimensional shape of the cluster along with the delocalization of each atom about its central

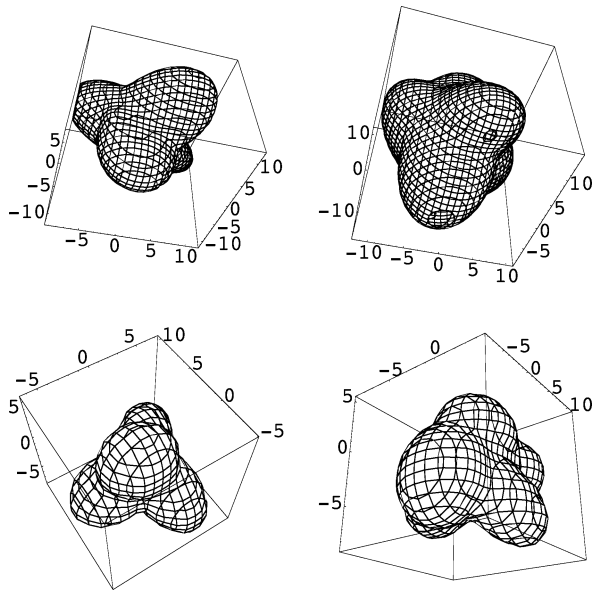

Figure 1. The isodensity contour plots of the clusters at a value of 0.006. In the upper left is the Ar_4 cluster, in the upper right is the Ne_4, lower left has the Ar_5, and then bottom right is Ne_5. The axes are listed in atomic units.

location. Each density "lobe" is nearly spherical with some elongation. These density plots give a suggestive view of the overlap of the densities, which is ignored in eqs 3 and 9. For the systems at hand, this overlap turns out to be minor, but for atoms such as Helium, this would have to be taken into account.

It has been noted in the literature[22] that lowering the mass, which results in increasing the quantum effects, will result in delocalization through the increase in the zero-point kinetic energy of the system. Under NPT conditions, this would result in two competing effects, the tendency to minimize the potential energy, and the tendency of the atoms to spread to minimize the quantum kinetic energy by increasing the volume. One expects a net volume increase as the nuclear ground-state wave function spreads out to minimize the quantum kinetic energy. This also leads to a net decrease in the binding potential energy because the atoms are effectively further apart. Also, there may be tunneling between mainly iso-energetic configurations separated by low-energy barriers. In summary, when quantum effects are present, the decrease in the binding potential energy and the quantum fluctuations lead to what is known as a softening of the crystal and a reduction of its melting temperature.

A similar interplay can be seen in the present method. In Figure 1, each atomic density has a finite width. This can be contrasted with the classical case that has δ functions representing the atoms. This spread is maintained by the kinetic energy term in the Hamiltonian through the quantum potential. In this sense, the quantum potential term is a measure of the quantum

TABLE 1: Interatomic Distances for X_5 Clusters in Angstroms

distances	argon	argon (cl)	neon	neon (cl)
$rd_{1,2}$	3.884 ± 0.010	3.822	3.262 ± 0.023	3.135
$rd_{1,3}$	3.875 ± 0.009	3.822	3.234 ± 0.016	3.135
$rd_{1,4}$	3.855 ± 0.009	3.808	3.204 ± 0.018	3.124
$rd_{1,5}$	3.845 ± 0.008	3.808	3.199 ± 0.014	3.124
$rd_{2,3}$	3.882 ± 0.012	3.822	3.259 ± 0.029	3.135
$rd_{2,4}$	3.849 ± 0.009	3.808	3.205 ± 0.020	3.124
$rd_{2,5}$	3.853 ± 0.008	3.808	3.211 ± 0.018	3.124
$rd_{3,4}$	3.843 ± 0.009	3.808	3.233 ± 0.031	3.124
$rd_{3,5}$	3.846 ± 0.008	3.808	3.214 ± 0.018	3.124
$rd_{4,5}$	6.259 ± 0.010	6.208	5.209 ± 0.020	5.092

TABLE 2: Interatomic Distances for X_4 Clusters in Angstroms

distances	argon	argon (cl)	neon	neon (cl)
$rd_{1,2}$	3.894 ± 0.012	3.814	3.262 ± 0.022	3.13
$rd_{1,3}$	3.859 ± 0.008	3.814	3.229 ± 0.026	3.13
$rd_{1,4}$	3.858 ± 0.010	3.814	3.222 ± 0.025	3.13
$rd_{2,3}$	3.872 ± 0.011	3.814	3.248 ± 0.020	3.13
$rd_{2,4}$	3.864 ± 0.008	3.814	3.214 ± 0.014	3.13
$rd_{3,4}$	3.854 ± 0.008	3.814	3.223 ± 0.021	3.13

character of the system and provides an intuitive way to understand softening of crystals.

In Figure 2, we show the total energy and the total potential energy for the Ar_5 and Ne_5 clusters as the system converges toward its lowest-energy state. Initially, there is a rapid restructuring of the densities as they adjust to find a close approximation to the actual ground-state density. Following this initial rapid convergence, there is slower convergence phase as the density is further refined. During this process, as the sample points look for a configuration that fully equalizes the quantum and kinetic energy terms from eq 6, the density approximation can sometimes prove inadequate and points can be pushed into temporary higher-energy regions. This leads to the fluctuations seen in the energies and any other averaged quantity such as the interatomic distances. To compute meaningful values for the energy and distances, we averaged these quantities over the last half million or so cycles. As can be seen from Figure 2, the Ne_5 cluster is slower to converge, but eventually does so after roughly 200 million iterations.

Tables 1 and 2 list the averaged interatom distances for each cluster compared to the equilibrium distances for the corresponding classical case. For the case of Ar_5, the numerical fluctuations lead to an uncertainly of about 0.3% in the interatomic distances and for Ne_5, a 0.5% uncertainty in the interatomic distances. These fluctuations are simply the root-mean-square of the values calculated. It is important to note that the fluctuations mentioned here tend to decrease with increasing system size, as can seen by comparing the results for Ar_5 with Ar_4. This has important implications because we hope to extend this method to larger systems. Ne_4 can be seen to have the largest fluctuations. This is expected because it is

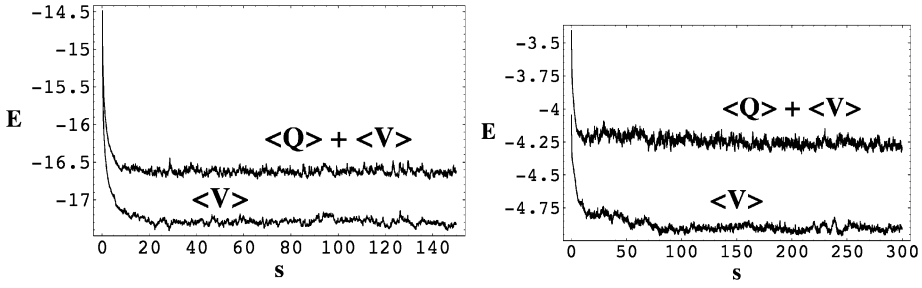

Figure 2. The average potential energy $\langle V \rangle$ and total energy $\langle Q \rangle + \langle V \rangle$ of the Ar_5 and Ne_5 clusters in kJ/mol. The steps are measured in millions.

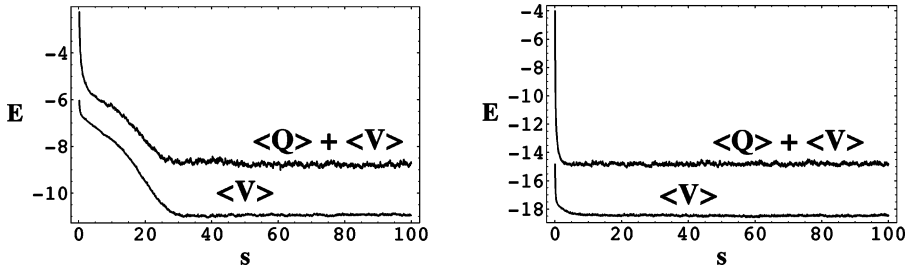

Figure 3. Convergence of the 13- and 19-atom clusters of neon. The energy is in kJ/mol and the steps are given in millions.

TABLE 3: Converged Ground-State Energies for 4- and 5-Atom Clusters in kJ/mol

	Ar_4	Ne_4	Ar_5	Ne_5
V_c	−5.986	−1.827	−9.083	−2.772
$\langle V\rangle$	−5.668 ± 0.112	−1.592 ± 0.028	−8.630 ± 0.114	−2.447 ± 0.117
$\langle Q\rangle$	0.462 ± 0.032	0.460 ± 0.034	0.689 ± 0.041	0.646 ± 0.036
$\langle E\rangle$	−5.205 ± 0.099	−1.132 ± 0.013	−7.940 ± 0.098	−1.801 ± 0.0005
E_0	0.781	0.695	1.143	0.971
$\langle Q\rangle/\langle\hat{V}\rangle$	0.082	0.288	0.079	0.263

the most quantum mechanical. All in all, these values compare well with the classical distances. In general, the quantum distances are slightly larger due to the fact that the Gaussian atom densities are sampling part of the anharmonic repulsive portion of the pair potential.

Table 3 summarizes the various contributions to the total energy for each cluster. The "classical" energies, V_c, are the energy minimum of the total potential energy surface corresponding to the classical equilibrium configuration, and they are obtained from the same code we used for the other quantum simulations but with $\hbar$ turned to zero. This corresponds to a classical molecular dynamics simulation, the implications of which are discussed later. $\langle V\rangle$, $\langle Q\rangle$, and $\langle E\rangle$ are the total quantum potential energy, kinetic energy, and total energy of each cluster, respectively. The difference between the classical potential minimum, V_c, and $\langle E\rangle$ is the zero-point energy, labeled E_0 in the table. One can see that the zero-point energies for the Ne_4 and Ne_5 systems account for 43.66 and 39.68%, respectively, of the total energy. We also calculate a virial-like term, which is the ratio of the kinetic to the potential energy of the system, $\langle Q\rangle/\langle\hat{V}\rangle$, where $\langle\hat{V}\rangle = \langle V\rangle - \langle V_0\rangle$. $\langle V_0\rangle$ is the limit of the potential energy at infinite separation. The kinetic term here is the quantum potential because the translational energy has been siphoned away. For larger systems, this ratio is expected to fall because the zero-point energy should become less important, and that is what is observed in the results.

In addition to the results for the small 4- and 5-atom clusters we have presented above, we also considered much larger 13- and 19-atom clusters of neon. These larger calculations are particularly challenging because the total number of degrees of freedom are considerably way beyond that which can be handled by standard grid-based techniques. These clusters correspond to the smallest "magic" number clusters that exist for Lennard−Jones systems and are particularly interesting because they have both interior (caged) and exterior (cage) atoms. The lowest-energy 13-atom cluster takes an icosahedral geometry with the 12 exterior atoms lying at the vertexes and the central caged atoms at the origin. Similarly, the 19-atom cluster is more of a prolate icosahedron with one extra band of 5 atoms and two interior atoms. Figure 4 shows the equilibrium positions of the atoms for both clusters. In performing the quantum calculations for these larger clusters, we used 200 sample points versus 300 used for the smaller clusters and used the equilibrium positions as staring points. In all other respects, the calculations proceeded as above.

TABLE 4: Converged Quantum Ground-State Energies of the Larger 13- and 19-Atom Clusters in kJ/mol

	Ne_{13}	Ne_{19}
V_c	−13.559	−22.226
$\langle V\rangle$	−10.928 ± 0.153	−18.472 ± 0.193
$\langle Q\rangle$	2.188 ± 0.081	3.651 ± 0.034
$\langle E\rangle$	−8.740 ± 0.099	−14.821 ± 0.133
E_0	4.819	7.405
$\langle Q\rangle/\langle\hat{V}\rangle$	0.200	0.197

The convergence with respect to total energy for the two larger neon clusters can be seen in Figure 3 with the final converged values given in Table 4. The large shoulder in the convergence of the 13-atom cluster was due to a small rearrangement of the atoms as the system relaxed. The virial term remains about the same as in the case of the smaller clusters. Furthermore, the zero-point energy for the clusters is 40.1% of the classical energy for the 19-atom cluster and 44.1% for the 13-atom cluster respectively. Also note that the V_c values for these larger clusters were obtained from the literature.[50−52]

Figure 4 also shows a snapshot of sample points for each cluster (2600 and 3800 points, respectively) in their lowest-energy quantum states. Recall that the classical sample points represent entire atoms, but the quantum sample points make up the quantum density "cloud" of each nuclei. In both cases, the quantum density of the interior atoms is more tightly compressed than the quantum density of the atoms on the surface of the cluster. Furthermore, notice that the mean position of the quantum atoms is farther away from the center of the cluster than in the classical case. Averaging over the exterior atoms, the quantum 13-atom cluster has a radius of 3.113 Å versus 3.017 Å for the classical case. This 3% increase in the radius results in nearly 20% increase in the volume of the cluster. A similar effect can be noted for the 19-atom cluster.

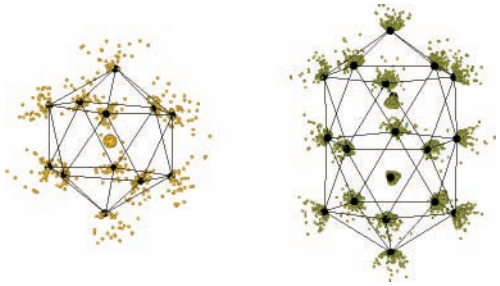

Figure 4. Thirteen and 19-atom clusters with the quantum sample points in yellow overlaid on the classical equilibrium positions in black.

This expansion has really two origins. First, quantum mechanical expectation value of the position $\langle r \rangle$ for any single atom will always be greater than the classical equilibrium position for any anharmonic and dissociative potential well. However, this does not wholly account for the 3% increase in mean radius. Rather, the increase is also due to the interior *quantum pressure* of the trapped atom pushing against the surrounding cage. The cage expands until the strain on the cage is equal and opposite the force exerted on the cage as the trapped atom's density expands.

If we consider the trapped atom as a particle in a spherical well with radius R, the pressure exerted on the walls is easily computed by using the reversible work theorem as $dW = PdV = 4\pi R^2 P dR = -dE(R)$, from which one can easily deduce that the quantum pressure of the trapped particle is[55]

$$P = \frac{\pi \hbar^2}{4mR^5}$$

Finally, if we take the actual well that the center Ne atom sits in from the surrounding 12 atoms to be quite steep with an effective hard-sphere radius of about 1 Å, we obtain an internal pressure of 0.013 kJmol^{-1} Å^{-1}. This small, but significant, outward force is sufficient to expand a 12-atom cluster by a small amount until the strain due to the expansion becomes large enough to counter the internal quantum pressure of the trapped atom.

VI. Discussion

A method for calculating ground-state configuration of quantum clusters and liquids has been outlined on the basis of some previous work in approximating densities as quantum statistical density functions. The quantum and the Lennard−Jones potentials are used to propagate an ensemble of Monte Carlo statistical points, in a DFT-like procedure. This is an orbital-free approach in the sense that we only work at the level of the nuclear density. To do this, we outline a "cluster" model and an expectation maximization (EM) algorithm that is used to obtain the density in terms of the statistical points representing each atom. The Lennard−Jones potential is calculated in a mean-field sense by averaging over the statistical points of each atom, and the quantum potential is calculated from the density obtained in the EM algorithm. Results were presented for 4-, 5-, 13-, and 19-atom clusters of argon and neon. The results indicate good agreement with the general classical results, but the quantum corrections can be seen to be significant.

The method outlined herein provides a means of artificial control of the amount of quantum mechanical information desired from a calculation. The covariances between the approximates representing atoms may be set to zero as we have done, but keeping the interatomic covariances seems to provide a possible path to including other effects such as exchange and correlation energies. This all comes at the expense of increased complexity and reduced computational speed.

The method also opens the fascinating possibility of using π as a parameter by which one can effectively *tune* the amount of quantum character given a specific atom. One can perform the equivalence of thermodynamic integration by considering the parametric dependence of the energy or structure of a system upon the transition from the fully quantum to the mixed quantum/classical regime. Additionally, one could surround one or many "quantum" particles with a bath of larger classical particles, which have $\hbar$ turned to zero and, therefore, are handled with standard molecular dynamics methods. This situation has each atom interacting in a mean-field sense so that the classical particles feel the pairwise potentials of the quantum mechanical particles "cloud" of sample points. So one can see that the present approach can be inserted or added as a subroutine into existing MD codes with relative ease. Then, by controlling $\hbar$, or which particles have quantum potentials, a variety of difficult systems could be modeled. We shall explore these issues in our forthcoming papers on this topic.

Acknowledgment. We would like to thank Jeremy Maddox for helpful discussions. This work was supported by grants from the National Science Foundation and the Robert Welch Foundation.

References and Notes

(1) Jellinek, J.; Beck, T. L.; Berry, R. S. *J. Chem. Phys.* **1986**, *84*, 2783.
(2) Zhang, C.; Berry, R. S. *J. Chem. Phys.* **2005**, *123*, 094103.
(3) Proykova, A.; Pisov, S.; Berry, R. S. *J. Chem. Phys.* **2001**, *115*, 8583.
(4) Last, I.; Jortner, J. *J. Chem. Phys.* **2004**, *120*, 1336.
(5) Predescu, C.; Frantsuzov, P. A.; Mandelshtam, V. A. *J. Chem. Phys.* **2005**, *122*, 154305.
(6) Berry, R. S. *J. Phys. Chem.* **1994**, *98*, 6910.
(7) Lynden-Bell, R. M.; Wales, D. J. *J. Chem. Phys.* **1994**, *101*, 1460.
(8) Calvo, F.; Doye, J. P. K.; Wales, D. J. *J. Chem. Phys.* **2001**, *114*, 7312.
(9) Chakravarty, C. *J. Chem. Phys. A* **1995**, *102*, 956.
(10) Chakravarty, C. *J. Chem. Phys. B* **1995**, *103*, 10663.
(11) Toda, R. K. M.; Saito, N. *Statistical Physics I: Equilibrium Statistical Mechanics*; Springer: Berlin, 1992).
(12) Zhang, D. H.; Zhang, J. Z. H. *J. Chem. Phys.* **1994**, *101*, 1146.
(13) Zhang, D. H.; Light, J. C. *J. Chem. Phys.* **1996**, *104*, 4544.
(14) Somers, M. F.; Olsen, R. A.; Busnengo, H. F.; Baerends, E. J.; Kroes, G. J. *J. Chem. Phys.* **2004**, *121*, 11379.
(15) Echave, J.; Clary, D. C. *J. Chem. Phys.* **1994**, *100*, 402.
(16) Guo, H.; Lao, K. Q.; Schatz, G. C.; Hammerich, A. D. *J. Chem. Phys.* **1991**, *94*, 6562.
(17) Manth, U.; Koppel, H. *Chem. Phys. Lett*. **1991**, *178*, 36.
(18) Manthe, U.; Meyer, H.-D.; Cederbaum, L. S. *Chem. Phys. Lett.* **1990**, *165*, 73.
(19) Manthe, U.; Meyer, H.-D.; Cederbaum, L. S. *J. Chem. Phys.* **1992**, *97*, 3199.
(20) Rick, S. W.; Leitner, D. L.; Doll, J. D.; Freeman, D. L.; Frantz, D. D. *J. Chem. Phys.* **1991**, *95*, 6658.
(21) Neirotti, J. P.; Freeman, D. L.; Doll, J. D. *J. Chem. Phys.* **2000**, *112*, 3990.
(22) Chakravarty, C. *J. Chem. Phys.* **2002**, *116*, 8938.
(23) Maddox, J. B.; Bittner, E. R. *J. Chem. Phys.* **2003**, *119*, 6465.
(24) Bloch, F. *Z. Phys*. **1928**, *81*, 263.
(25) Runge, E.; Gross, E. K. U. *Phys. Rev. Lett.* **1984**, *52*, 997.
(26) Banerjee, A.; Harbola, M. K. *J. Chem. Phys.* **2000**, *113*, 5614.
(27) Banerjee, A.; Harbola, M. K. *J. Chem. Phys.* **2002**, *117*, 7845.
(28) Parr, R. G.; Yang, W. *Density Functional Theory of Atoms and Molecules*; Clarendon Press: New York; Oxford University Press: Oxford, U.K., 1989.
(29) Madelung, E. *Z. Phys.* **1926**, *40*, 322.
(30) de Broglie, L. *C. R. Acad. Sci. Paris* **1926**, *183*, 447.
(31) de Broglie, L. *C. R. Acad. Sci. Paris* **1927**, *184*, 273.
(32) Holland, P. R. *The Quantum Theory of Motion*; Cambridge University Press: New York, 1993).
(33) Bohm, D. *Phys. Rev. A* **1952**, *85*, 166.
(34) Bohm, D. *Phys. Rev. B* **1952**, *85*, 180.
(35) Bohm, D.; Hiley, B. J.; Kaloyerou, P. N. *Phys. Rep*. **1987**, *144*, 321.
(36) Wyatt, R. E. *Chem. Phys. Lett.* **1999**, *313*, 189.
(37) von Weizsacker, C. F. *Z. Phys*. **1935**, *96*, 431.
(38) Gershenfeld, N. *The Nature of Mathematical Modeling*; Cambridge University Press: Cambridge, U.K., 1999.
(39) McLachlan, G. J.; Basford, K. E. *Mixture Models: Inference and Applications to Clustering*; Dekker: New York, 1988.
(40) Heller, E. J. *J. Chem. Phys.* **1981**, *75*, 2923.
(41) Xu, L.; Jordan, M. I. *Neural Comput.* **1996**, *8*, 129.
(42) Garashchuk, S.; Rassolov, V. A. *J. Chem. Phys.* **2003**, *118*, 2482.
(43) Garashchuk, S.; Rassolov, V. A. *Chem. Phys. Lett*. **2002**, *364*, 562.
(44) Lopreore, C.; Wyatt, R. E. *Phys. Rev. Lett.* **1999**, *82*, 5190.
(45) Kendrick, B. K. *J. Chem. Phys.* **2003**, *119*, 5805.
(46) Wyatt, R. E.; Bittner, E. R. *J. Chem. Phys.* **2000**, *113*, 8898.
(47) Hughes, K. H.; Wyatt, R. E. *Chem. Phys. Lett.* **2002**, *366*, 336.

(48) Wyatt, R. E. *Quantum Dynamics With Trajectories*, 1st ed.; Springer Science + Business Media: New York, 2005.
(49) Lively, D. M. *J. Phys. C: Solid State Phys*. **1983**, *16*, 2889.
(50) Hoare, M. R.; Pal, P. *Adv. Phys. A* **1971**, *20*, 161.
(51) Hoare, M. R.; Pal, P. *Nature (London) Phys. Sci.* **1971**, *230B*, 5.
(52) Hoare, M. R.; Pal, P. *Nature (London) Phys. Sci.* **1972**, *236*, 35.
(53) It is straightforward to show that, for the eigenstates, the quantum potential is given by $Q_n(x) = ((n + {}^1/_2)\hbar\omega) - ({}^1/_2 m\omega^2 x^2)$. Hence, for any eigenstate, the quantum potential is simply $-V(x)$ shifted by its energy eigenvalue, and once the $\nabla\phi = 0$ condition is met, there are no net forces.
(54) http://eiger.chem.un.edu:8080/webMathematics/pchem-apps/Plot3DLive.jsp.
(55) This is an elementary problem. Take $\psi(r) = (\sin(kr))/(kr)$ and the boundary condition $\psi(R) = 0$. Solving the Schrödinger equation gives $E(R) = (k^2\hbar^2)/(2mR^2)$.